Journal of Computer Science and Cybernetics, V.36, N.2 (2020), 187–204
DOI 10.15625/1813-9663/36/2/14807

DESIGNING A ROBUST ADAPTIVE TRACKING CONTROLLER CONSIDERING ACTUATOR SATURATION FOR A WHEELED MOBILE ROBOT TO COMPENSATE UNKNOWN SLIPPAGE

CHUNG LE[1,*], KIEM NGUYEN TIEN[2], LINH NGUYEN[3], TINH NGUYEN[4], TUNG HOANG[4]

[1]*Faculty of Automation Technology, Thai Nguyen University of Information and Communication Technology*

[2]*Faculty of Electronics Engineering Technology, Hanoi University of Industry, Hanoi, Vietnam*

[3]*Faculty of Control and Automation, Electric Power University, Hanoi, Vietnam*

[4]*Institute of Information Technology, Vietnam Academy of Science and Technology*

Abstract. This article highlights a robust adaptive tracking control approach for a nonholonomic wheeled mobile robot by which the bad problems of both unknown slippage and uncertainties are dealt with. The radial basis function neural network in this proposed controller assists unknown smooth nonlinear dynamic functions to be approximated. Furthermore, a technical solution is also carried out to avoid actuator saturation. The validity and efficiency of this novel controller, finally, are illustrated via comparative simulation results.

Keywords. Actuator saturation; Nonholonomic; Wheeled mobile robot; Unknown slippage.

1. INTRODUCTION

Nowadays, it is well acknowledged that designing controllers for wheeled mobile robots (WMRs) is strongly appealing to researchers throughout the world. The reason is that each WMR has a wide range of action, which creates a favorable condition for its applicability to be increasingly prevalent. Thus, significantly more WMRs have been applied in a variety of practical applications than ever before. Such practical applications might be in military operations, transportation, rescue, observation, and so forth.

Thanks to the remarkable improvement of the science and engineering in the control field, there have been a great number of reports in the literature showing various control methods for WMRs. For instance, the authors in [1] have proposed a robust adaptive tracking control method for WMRs. The work [2] revealed a suggestion of an adaptive PID sliding mode controller based on a neural network in order to control a nonholonomic WMR. The study [3] tackled a tracking control problem in polar coordinates for a nonholonomic WMR via a sliding mode control method. A tracking control method utilizing input-output linearization was proposed in [4]. An adaptive control approach of an electrically driven nonholonomic WMR through backstepping and fuzzy techniques was published in [5]. Such reports were based on an assumption that wheels' motion is pure rolling without slippage, that is to say, the WMRs' nonholonomic constraint is always satisfied.

*Corresponding author.
E-mail addresses: lvchung@ictu.edu.vn (C.Le); kiemnt@haui.edu.vn (K.T.Nguyen); linhnt@epu.edu.vn (L.Nguyen); nvtinh@ioit.ac.vn (T.Nguyen); htung.avt@ioit.ac.vn (T.Hoang).

Nevertheless, the no-slip assumption is possibly violated in many practical applications due to slippery and irregular surface, centrifugal force as soon as a WMR moves in a circular path, and so on [6]. In other words, there may exist slippage between the wheels and the floor. It is because of slippage that the performance of closed-loop control systems for WMRs deteriorates [7, 8, 9, 10, 11]. As a consequence, necessary steps must be taken in order to combat some reduction in tracking control performance due to slippage [12].

Of course, there have been researches addressing the slippage for a WMR. In particular, in 2006, a linearized kinematic model-based robust controller for car-like mobile robots was shown in [13]. In [14], thanks to extending the framework of the differential flatness theory to the models with slip uncertainties, robust trajectory-tracking controllers for differential driven two-wheeled mobile robots were developed via taking account of not only the dynamic but also kinematic model with slippage. In [15] released in 2012, a nonlinear disturbance observer was adopted with the purpose of estimating a nonlinear disturbance term involving both lateral and longitudinal slip. Next, the same author extended such a work to an obstacle avoidance problem [16] with not only slippage but also actuator saturation. In 2013, a robust tracking controller based on a Generalized Extended State Observer for a WMR badly affected by unknown skidding and slipping was proposed by [17]. In [18] published in 2014, the overall dynamics of a WMR subject to wheel slips has been considered as an under-actuated nonlinear dynamic system. After that, control algorithms in not only regulation but also turning tasks were proposed for the WMR.

Taking everything into consideration, most of these above control methods have not addressed the tracking control problem in the body coordinate system which is attached to the platform of a WMR, or, more precisely, they were designed in the global coordinate system except for [7, 8, 9, 10, 11]. As a consequence, an estimator for obtaining sideslip angle (see Figure 1) [19, 20] or an observer estimating the model of friction [21, 22] must be needed for designing such controllers. In accordance with the assessment of [23] published in 2008, it is difficult and/or expensive to estimate the sideslip angle as well as the coefficient of friction, even though fundamental variables such as linear acceleration, linear velocity, yaw rate can be easily measured by means of affordable sensors.

In this article, the proposed control approach will confront the serious issue of slippage under the body coordinate system, which is similar to [7, 8, 9, 10, 11]. As a result, observers for estimating both the sideslip angle and the friction coefficient are not required anymore.

When it comes to actuator saturation as can be seen from Figure 2, one must remember that it is one of the most common nonlinear factors in control systems. It exists due to the fact that every actuator has a torque limitation. Once a controller demands a great torque that exceeds such a limitation, the control performance goes down [24]. Designing controllers considering actuator saturation, hence, has been widely conducted all over the world and there have been many scientific reports in the literature about this problem [25]. There is a broad recognition that methods tackling actuator saturation are divided into two major groups: ONE-STEP and TWO-STEP [26]. In particular, the one-step approach simultaneously performs both designing a control law which meets all nominal specifications of a desirable control performance and handling actuators' constraints. Even though this approach is acceptable in theory, it has still lacked applicability to several practical tasks [27]. Meanwhile, the two-step approach firstly designs the pure control law without taking account of actuators' saturation. Subsequently, a saturation compensator such as an anti-

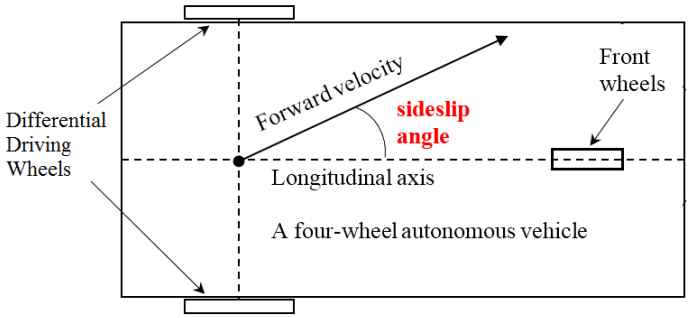

Figure 1. Slipside angle [10]

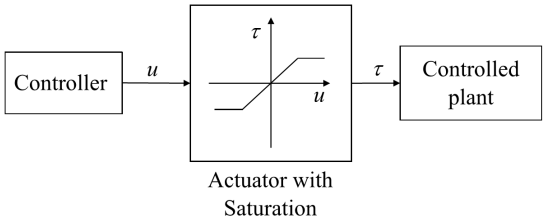

Figure 2. Actuator saturation

windup compensator must be utilized so as to minimize the bad influence of the actuator saturation on the control performance of a closed-loop control system once it happens. As opposed to the one-step approach, the two-step one becomes more prevalent. An explanation is that the latter permits practical engineers to design controllers without restriction, followed by retrofitting a saturation compensator. Nonetheless, the disadvantage of the latter is that they must also rapidly remove the output of the saturation compensator as soon as actuator saturation stops happening [28].

Although our proposed control approach indirectly avoids the actuator saturation in the one-step way, thanks to our novel technical solution, its applicability to several practical problems will be enhanced significantly.

The contributions of this paper are composed of the two new findings as following:

- Designing a robust tracking controller, which is carried out in order to simplify the algorithm in Chapter 4 of [10]. Therefore, the burden of computation will be also reduced remarkably.

- As opposed to [7, 8, 9, 11], a technical solution is used to indirectly avoid actuator saturation and then making this controller suitable for physical limitations in practical applications.

The structure of this paper is organized as follows. Section 2 shows preliminaries comprising the kinematics and dynamics of the WMR with slippage, followed by the description of a RBFNN. Section 3 reveals the problem description, the robust kinematic control law, the

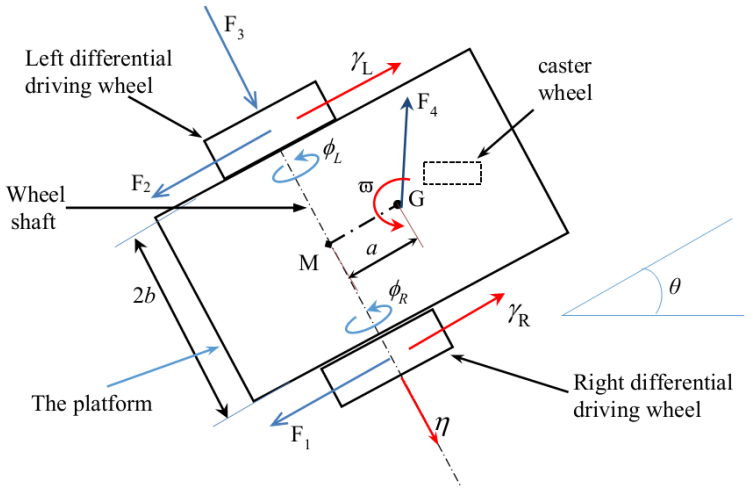

Figure 3. The nonholonomic WMR subjected to unknown slippage

robust adaptive dynamic control law, and the stability analysis. Computer simulation results are clearly shown in Section 4 in order to confirm the validity and efficiency of this proposed control method. Finally, our conclusions are described in Section 5.

2. PRELIMINARIES

2.1. Kinematic model of a WMR subjected to slippage

Figure 3 is a clear illustration of a nonholonomic WMR composed of two differential driving wheels and a passive wheel. $G(x_G, y_G)$, namely, is an illustration of the platform's mass centroid. Likewise, the wheel-shaft's midpoint is shown by $M(x_m, y_m)$. Next, F_1, F_2 and F_3, respectively depict the illustrations of the friction forces between the driving wheels and the floor along the corresponding directions. F_4 and ϖ are expressions of an external force and moment acting on G, respectively. If there is no slip between the floor and the driving wheels, then the two following conditions will be always fulfilled:

- The orientation of the linear velocity is always assured to be perpendicular to the wheelshaft, or, more precisely, the sideslip angle (see Figure 1) always equals to zero.
- Both the velocities and accelerates of the WMR's platform comprehensively depend on the pure rolling motion of the two differential driving wheels.

If the WMR works in the presence of slippage, then the actual linear velocity of the WMR along the longitudinal direction will be expressed in the following illustration [7, 8, 9, 10, 11]

$$\vartheta = \frac{r\left(\dot{\phi}_R + \dot{\phi}_L\right)}{2} + \frac{\dot{\gamma}_R + \dot{\gamma}_L}{2}, \tag{1}$$

where ϕ_R and ϕ_L respectively representing the angular coordinates of the right and left differential driving wheels about the wheel-shaft axis; $\dot{\gamma}_R$ and $\dot{\gamma}_L$ respectively are the longi-

tudinal slip velocities of the right and left wheels; r denotes the radius of each driving wheel. Likewise, the actual yaw rate is also computed as follows [7, 8, 9, 10, 11]

$$\omega = \frac{r\left(\dot{\phi}_R - \dot{\phi}_L\right)}{2b} + \frac{\dot{\gamma}_R - \dot{\gamma}_L}{2b} \tag{2}$$

with b showing a half of the wheel-shaft.

Let $\dot{\eta}$ be the lateral slippage velocity of this WMR along the wheel-shaft (see Figure 1.). The kinematics, as a consequence, can be expressed as follows

$$\begin{cases} \dot{x}_M &= \vartheta \cos\theta - \dot{\eta}\sin\theta \\ \dot{y}_M &= \vartheta \sin\theta + \dot{\eta}\cos\theta \\ \dot{\theta} &= \omega. \end{cases} \tag{3}$$

The perturbed nonholonomic constrains can in turn be written as follows [15]

$$\begin{cases} \dot{\gamma}_R &= -r\dot{\phi}_R + \dot{x}_M\cos\theta + \dot{y}_M\sin\theta + b\omega \\ \dot{\gamma}_L &= -r\dot{\phi}_L + \dot{x}_M\cos\theta + \dot{y}_M\sin\theta - b\omega \\ \dot{\eta} &= -\dot{x}_M\sin\theta + \dot{y}_M\cos\theta. \end{cases} \tag{4}$$

2.2. The dynamic model of a WMR considering slippage

Applying Euler-Lagrange formulation, the dynamics of this WMR, which is similar to [7, 8, 9, 10, 11] is shown in the following equation

$$\mathbf{M}\dot{\mathbf{v}} + \mathbf{B}(\mathbf{v})\mathbf{v} + \boldsymbol{\tau}_{\mathrm{d}} = \boldsymbol{\tau}, \tag{5}$$

where $\boldsymbol{\tau} = [\tau_R, \tau_L]^{\mathrm{T}}$ is the input vector with τ_R and τ_L respectively showing the torques at the right and left differential driving wheel about the wheel shaft; τ_d is the description of an unknown vector including the bad influence of the slippage, the model uncertainties (due to the variation and no prior knowledge of dynamic parameters); $\mathbf{v} = \left[\dot{\phi}_R,\ \dot{\phi}_L\right]^T$ is the angular velocities of the differential driving wheels about their rotational axis; $\mathbf{M}$ is the inertial matrix; $\mathbf{B}$ is the centrifugal and Coriolis matrix.

Property 1. $\mathbf{M}$ is always invertible, differential, positive-definite, symmetric, and bounded such that $M_1\|\mathbf{x}\|^2 \leq \mathbf{x}^{\mathrm{T}}\mathbf{M}\mathbf{x} \leq M_2\|\mathbf{x}\|^2\ \forall\mathbf{x} \in \mathrm{R}^{2\times 1}$ where M_1, and M_2 are known positive constants.

Property 2. $\dot{\mathbf{M}} - 2\mathbf{B}$ is a skew-symmetric matrix. It implies that $\mathbf{x}^{\mathrm{T}}(\dot{\mathbf{M}} - 2\mathbf{B})\mathbf{x} = 0$ $\forall\mathbf{x} \in \mathbf{R}^{2\times 1}$.

2.3. Radial basis function neural network

Evidently, no prior knowledge of the dynamics of controlled plants has been one of the most popular reasons why unknown nonlinear smooth functions have existed. Such functions need to be approximated so as to enhance the control performance. The radial basis function neural network (RBFNN) is one of the most prevalent tools making approximations easier.

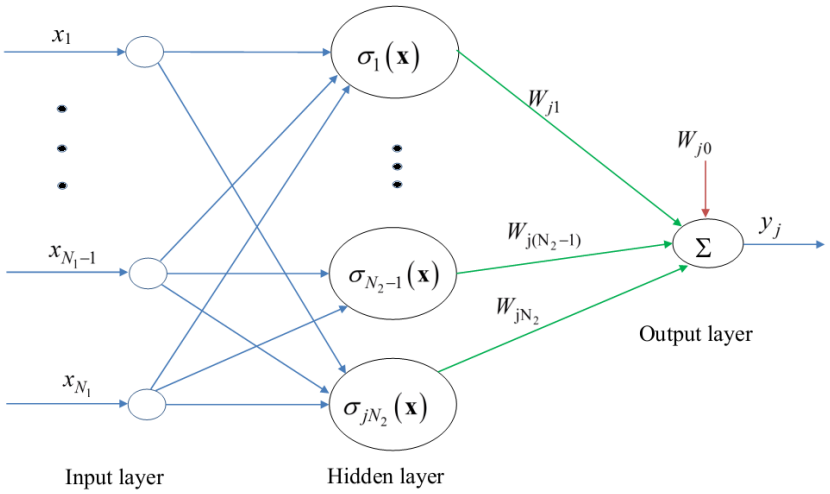

Figure 4. The diagram of RBFNN

It has, therefore, been applied in various areas of the control theory and engineering. For instance, the authors in [12] have utilized this RBFNN to make an approximation of such unknown smooth dynamic functions of the WMR.

According to [10], the illustration of such a RBFNN will be briefly expressed in this subsection. Overwhelmingly, what stands out from Figure 4 is that its structure is composed of 3 layers: The input, hidden, and output layers.

In particular, the input layer is revealed by $\mathbf{x} = [x_1, \cdots, x_{N_1}]^{\mathrm{T}}$ with N_1 showing the number of the input-layer neurons. In the hidden layer, there are N_2 activation functions. It is, in this work, suitable to select every activation function as a Gaussian type function as follows

$$\sigma_i(\mathbf{x}) = \exp\left(\frac{1}{2\psi_i^2}\|\mathbf{x} - \xi_i\|^2\right) \text{ with } i = 1, \ldots, N_2, \tag{6}$$

where ξ_i and ψ_i respectively show the illustrations of the center and width of the Gaussian function of the i -th hidden-layer neuron.

When it comes to the output layer, it is formed via a linear combination of the weights and such activation functions. Interestingly, the illustration of the j -th output-layer neuron is expressed as follows

$$y_j = W_{j0} + \sum_{i=0}^{N_2} W_{ji}\sigma_i(\mathbf{x}) \text{ with } j = 1, \cdots, N_3, \tag{7}$$

where, N_3 is the number of the output neurons.

Here, one striking feature is that W_{j0} shows the illustration of the threshold offset of the j-th outputlayer neuron. The neural network (NN) weight W_{ji} makes a link between the j-th output-layer neuron and the i-th hidden-layer one. For convenience in description, one can rewrite (7) in terms of vector as follows

$$\mathbf{y}(\mathbf{x}) = \mathbf{W}^{\mathrm{T}}\boldsymbol{\sigma}(\mathbf{x}), \tag{8}$$

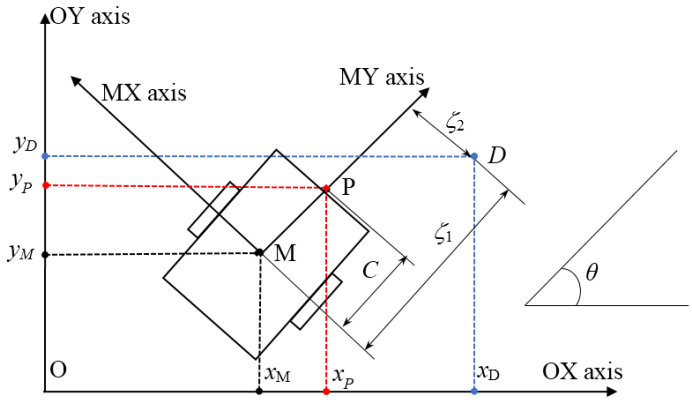

Figure 5. The representation of target D in the body frame M-XY

where $\mathbf{y}(\mathbf{x}) = [y_1, \cdots, y_{N_3}]^{\mathrm{T}}$, $\sigma(\mathbf{x}) = [1, \sigma_1, \cdots, \sigma_{N_2}]^{\mathrm{T}}$, $\mathbf{W}$ is constituted by not only the weights W_{jt} but the threshold offsets W_{j0} also.

Assumption 1. $\mathbf{W}$ is bounded by a known positive real constant value. To be specific, let W_M be a known upper bound of $\mathbf{W}$, which implies that $\|\mathbf{W}\|_{\mathrm{F}} \leq W_{\mathrm{M}}$ with $\|\mathbf{W}\|_{\mathrm{F}}$ denoting the Frobenius norm [12] of $\mathbf{W}$.

For any a bounded and continuous function vector $\mathbf{f}(\mathbf{x}) : \mathbf{R}^{N_1 \times 1} \to \mathbf{R}^{N_3 \times 1}$, there exists an optimal matrix $\overline{\mathbf{W}}$ such that

$$\mathbf{f}(\mathbf{x}) = \mathbf{y}(\mathbf{x}) + \boldsymbol{\varepsilon} = \overline{\mathbf{W}}^T \boldsymbol{\sigma} + \boldsymbol{\varepsilon}, \tag{9}$$

where ε is the vector of reconstruction errors. For convenience in description, we denote $\boldsymbol{\sigma} = \boldsymbol{\sigma}(\boldsymbol{x})$.

Assumption 2. The reconstruction error vector ε is bounded by a positive constant value ε_{M}. In other words, we can write that $\|\boldsymbol{\varepsilon}\| \leq \varepsilon_{\mathrm{M}}$.

Let $\hat{\mathbf{W}}$ be the actual weight matrix of the RBFNN in order to approximate $\mathbf{f}(\mathbf{x})$ in (9). One can write a good approximation of $\mathbf{f}(\mathbf{x})$ as follows

$$\hat{\mathbf{f}}(\mathbf{x}) = \hat{\mathbf{W}}^{\mathrm{T}} \sigma. \tag{10}$$

3. DESIGNING THE CONTROL SYSTEM

3.1. Problem description

The control goal is to look for an adaptive tracking controller considering actuator saturation for a WMR to cope with the unknown wheel slip such that the point P of the WMR (see Figure 6) coincides with the target D with a desired tracking control performance.

Remark 1. According to [10] due to the fact that the nonholonomic constraint (4) stops M converging to D along MX axis in the body frame M-XY (see Figure 5), the control goal is to make point P (instead of M) coincide with the target D.

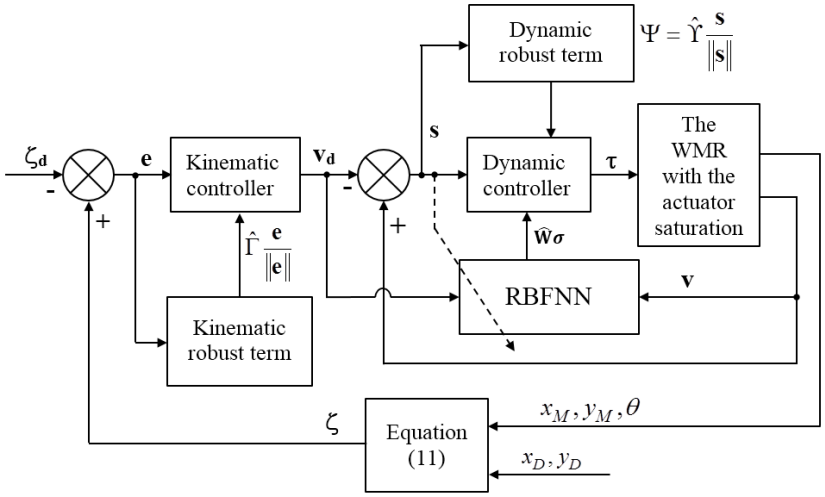

Figure 6. The diagram of entire control system

According to [10], to solve this problem the overall diagram of the control system is shown as Figure 6.

3.2. The robust kinematic control law

Firstly, the position of target D is shown in the body frame M-XY (see Figure 5) as follows

$$\zeta = \begin{bmatrix} \zeta_1 \\ \zeta_2 \end{bmatrix} = \begin{bmatrix} \cos\theta & \sin\theta \\ -\sin\theta & \cos\theta \end{bmatrix} \begin{bmatrix} x_D - x_M \\ y_D - y_M \end{bmatrix}, \tag{11}$$

where (x_D, y_D) is the postion of D in the world frame O-XY.

Assumption 3. Both x_D and y_D are bounded and twice differentiable

Differentiating (11) then yields

$$\dot{\zeta} = \mathbf{hv} + \begin{bmatrix} \cos\theta & \sin\theta \\ -\sin\theta & \cos\theta \end{bmatrix} \begin{bmatrix} \dot{x}_D \\ \dot{y}_D \end{bmatrix} + \chi, \tag{12}$$

where $\mathbf{h} = \begin{bmatrix} \left(\frac{\zeta_2}{b} - 1\right)\frac{r}{2} & -\left(\frac{\zeta_2}{b} + 1\right)\frac{r}{2} \\ -\frac{\zeta_1 r}{2b} & \frac{\zeta_1 r}{2b} \end{bmatrix}$ and $\chi = -\begin{bmatrix} \frac{\dot{\gamma}_R + \dot{\gamma}_L}{2} \\ \dot{\eta} \end{bmatrix} + \frac{\dot{\gamma}_R - \dot{\gamma}_L}{2b}\begin{bmatrix} \zeta_2 \\ -\zeta_1 \end{bmatrix}$.

Assumption 4. All slip velocities $\dot{\gamma}_R$, $\dot{\gamma}_L$ and $\dot{\eta}$ are bounded. As a result, there exists a certain positive real constant value Γ such that$\|\mathbf{x}\| \leq \Gamma$.

Remark 2. By virtue of $\det(\mathbf{h}) = \frac{\zeta_1 r^2}{2b}$, $\mathbf{h}$ is invertible as long as $\zeta_1 \neq 0$.

According to the aforementioned control goal in Subsection 3.1 and Figure 5, it is appropriate to select the desired vector ζ as $\xi_{\mathrm{d}} = \begin{bmatrix} C \\ 0 \end{bmatrix}$. Therefore, the vector of the position

tracking errors in the body frame M-XY is defined by

$$\mathbf{e} = \begin{bmatrix} e_1 \\ e_2 \end{bmatrix} = \zeta - \zeta_d. \tag{13}$$

It is obvious that χ is unknown. If the condition $\zeta_1 \neq 0$ is met (see Remark 2), then a possible kinematic control law will be suggested as follows

$$\mathbf{v}_{\mathrm{d}} = \mathbf{h}^{-1}\left(-\Lambda\mathbf{e} - \begin{bmatrix} \cos\theta & \sin\theta \\ -\sin\theta & \cos\theta \end{bmatrix}\begin{bmatrix} \dot{x}_D \\ \dot{y}_D \end{bmatrix} - \hat{\Gamma}\frac{\mathbf{e}}{\|\mathbf{e}\|}\right), \tag{14}$$

where Λ is a symmetric positive-definite matrix and can be arbitrarily selected; $\hat{\Gamma}$ the kinematic robust gain online updated as the following equation

$$\dot{\hat{\Gamma}} = \mathrm{H}\|\mathbf{e}\|, \tag{15}$$

where H denotes a positive real constant and can be chosen in an arbitrary way. Substitution of $\mathbf{v}$ in (12) by $\mathbf{v}_{\mathrm{d}}$ in (14) results in

$$\dot{\mathbf{e}} = -\Lambda\mathbf{e} + \chi - \hat{\Gamma}\frac{\mathbf{e}}{\|\mathbf{e}\|}. \tag{16}$$

3.3. The robust adaptive dynamic control law

An unknown smooth nonlinear dynamic function vector, first of all, is defined as the following form

$$\mathbf{f}(\mathbf{x}) = -\mathbf{M}\dot{\mathbf{v}}_{\mathrm{d}} - \mathbf{B}(\mathbf{v})\mathbf{v}_{\mathrm{d}} \tag{17}$$

with $\mathbf{x} = \left[\mathbf{v}^{\mathrm{T}}, \mathbf{v}_{\mathrm{d}}^{\mathrm{T}}, \dot{\mathbf{v}}_{\mathrm{d}}^{\mathrm{T}}\right]^{\mathrm{T}}$ being the input of the RBFNN and easily measured.

Adding $\mathbf{f}(\mathbf{x})$ to the both sides of (5) results in

$$\mathbf{M}\dot{\mathbf{s}} = \boldsymbol{\tau} + \mathbf{f}(\mathbf{x}) - \mathbf{B}\mathbf{s} - \boldsymbol{\tau}_{\mathbf{d}} \tag{18}$$

with $\mathbf{s} = \mathbf{v} - \mathbf{v}_{\mathbf{d}}$ presenting the vector of the angular velocity tracking errors.

Owing to the fact that there is no perfect knowledge of the dynamics of the WMR, it is impossible to exactly know $\mathbf{f}(\mathbf{x})$. Let us, hence, propose the dynamic control law as follows

$$\boldsymbol{\tau} = -\mathbf{K}\cdot\mathrm{sgn}(\mathbf{s}) - \hat{\mathbf{f}}(\mathbf{x}) - \hat{\gamma}\frac{\mathbf{s}}{\|\mathbf{s}\|}, \tag{19}$$

where $\hat{\mathbf{f}}(\mathbf{x})$ is the output of the RBFNN described by (10) and is employed so as to estimate $\mathbf{f}(\mathbf{x})$; $\mathbf{K}$ is a positive-definite diagonal constant matrix, and further it can be arbitrarily chosen; $\mathbf{sgn}(\mathbf{s}) = \left[|s_1|^{\alpha}\,\mathrm{sign}\,(s_1)\,|s_2|^{\alpha}\,\mathrm{sign}\,(s_2)\right]^{\top}$ helps the dynamic controller avoid the actuator saturation; α is a positive real constant selected in an arbitrary way meeting $\alpha < 1$. Next, $\hat{\gamma}$ is the dynamic robust gain updated online as

$$\dot{\hat{\gamma}} = \mathrm{P}\|\mathbf{s}\| \tag{20}$$

with P being an arbitrary positive constant. Substituting (9), (10) and (19) into (18), leads to

$$\mathbf{M}\dot{\mathbf{s}} = -\mathbf{K}\cdot\mathbf{sgn}(\mathbf{s}) - \mathbf{B}\mathbf{s} + \tilde{\mathbf{W}}\sigma - \hat{\gamma}\frac{\mathbf{s}}{\|\mathbf{s}\|} + \mathbf{d}, \tag{21}$$

where $\mathbf{d} = \boldsymbol{\varepsilon} - \boldsymbol{\tau}_{\mathrm{d}}$ is the total uncertainty term; $\tilde{\mathbf{W}} = \overline{\mathbf{W}} - \hat{\mathbf{W}}$.

Assumption 5. The total uncertainty term in (21) is bounded as the following inequality

$$\|\mathbf{d}\| \leq \Upsilon \tag{22}$$

with Υ indicating a certain positive constant.

Let us propose an online weight updating law of the RBFNN via measurable signals in $\mathbf{x}$ and $\mathbf{s}$ as follows

$$\dot{\hat{\mathbf{W}}} = -\mathbf{Q}\boldsymbol{\sigma}\mathbf{s}^{\mathrm{T}}, \tag{23}$$

where $\mathbf{Q}$ is a diagonal, positive-definite constant matrix and can be arbitrarily selected.

3.4. Stability analysis

Theorem 1. *Let us take the WMR into account in the presence of the unknown wheel slips, model uncertainties, and actuator saturation. To be more specific, its kinematics and dynamics are represented by* (3) *and* (5)*, respectively. Let Assumptions 1-5 be met.*

If the proposed control scheme as shown in Figure 6 is utilized, which is constructed from the kinematic control law (14)*, the dynamic control law* (19)*, and online updating laws* (15)*,* (20)*, and* (23)*, then both the position and angular velocity tracking error vector, e and s, will converge to zero as* $t \to \infty$.

Proof. Let us choose a Lyapunov candidate function in the form

$$V(t) = \frac{1}{2}\mathbf{e}^{\mathrm{T}}\mathbf{e} + \frac{1}{2}\mathbf{s}^{\mathrm{T}}\mathbf{M}\mathbf{s} + \frac{1}{2}\,\mathrm{tr}\left(\tilde{\mathbf{W}}^{\mathrm{T}}\mathbf{Q}^{-1}\tilde{\mathbf{W}}\right) + \frac{1}{2}\mathrm{H}^{-1}\tilde{\Gamma}^2 + \frac{1}{2}\mathrm{P}^{-1}\tilde{\gamma}^2, \tag{24}$$

where, tr(.) denotes the trace of a matrix; $\tilde{\Gamma} = \Gamma - \hat{\Gamma}$; $\tilde{\Upsilon} = \Upsilon - \hat{\Upsilon}$ (see Assumptions $4-5$). Taking the first derivative of (24) with noting that $\dot{\tilde{\Gamma}} = -\dot{\hat{\Gamma}}$; $\dot{\tilde{\Upsilon}} = -\dot{\hat{\Upsilon}}$; $\dot{\tilde{\mathbf{W}}} = -\dot{\hat{\mathbf{W}}}$, it follows that

$$\dot{V} = \mathbf{e}^{\mathrm{T}}\dot{\mathbf{e}} + \mathbf{s}^{\mathrm{T}}\mathbf{M}\dot{\mathbf{s}} + \frac{1}{2}\mathbf{s}^{\mathrm{T}}\dot{\mathbf{M}}\mathbf{s} - \mathrm{tr}\left(\tilde{\mathbf{W}}^{\mathrm{T}}\mathbf{Q}^{-1}\dot{\mathbf{W}}\right) - \mathrm{H}^{-1}\tilde{\Gamma}\dot{\tilde{\Gamma}} - \mathrm{P}^{-1}\tilde{\gamma}\dot{\tilde{\gamma}}. \tag{25}$$

Substitution of (15), (16), (20), (21) and (23) into (25) with noting both Property 2 and $\mathrm{tr}\left(\tilde{\mathbf{W}}^{\mathrm{T}}\boldsymbol{\sigma}\mathbf{s}^{\mathrm{T}}\right) = \mathbf{s}^{\mathrm{T}}\tilde{\mathbf{W}}^{\mathrm{T}}\boldsymbol{\sigma}$ leads to

$$\dot{V} = -\mathbf{e}^{\mathrm{T}}\Lambda\mathbf{e} + \mathbf{e}^{\mathrm{T}}\chi - \hat{\Gamma}\|\mathbf{e}\| - \mathbf{s}^{\mathrm{T}}\mathbf{K}\cdot\mathbf{sgn}(\mathbf{s}) + \mathbf{s}^{\mathrm{T}}\mathbf{d} - \hat{\gamma}\|\mathbf{s}\| - \tilde{\Gamma}\|\mathbf{e}\| - \tilde{\gamma}\|\mathbf{s}\|. \tag{26}$$

In the light of Assumptions 4-5, one can write the following inequality

$$\dot{V} \leq -\mathbf{e}^{\mathrm{T}}\Lambda\mathbf{e} - \mathbf{s}^{\mathrm{T}}\mathbf{K}\cdot\mathbf{sgn}(\mathbf{s}). \tag{27}$$

It is clear that $\dot{V} \leq 0\ \forall \mathbf{e},\ \mathbf{s} \in \mathbf{R}^{2\times 1}$. This implies that $V(t) \leq V(0)$. Consequently, all $\mathbf{e}$, $\mathbf{s}$, $\tilde{\mathbf{W}}$, $\tilde{\Gamma}$, $\tilde{\gamma}$ are bounded for all $t > 0$ as long as they all were bounded at the initial time $t = 0$. Thanks to applying Lyapunov criteria, the whole control system is certainly concluded to be stable.

In order to demonstrate the asymptotic convergence of both $\mathbf{e}$ and $\mathbf{s}$ to zero, let us define another Lyapunov candidate function as follows

$$V_2(t) = V(t) - \int_0^t \left[V(\xi) + \mathbf{e}^{\mathrm{T}}(\xi)\Lambda\mathbf{e}(\xi) + \mathbf{s}^{\mathrm{T}}(\xi)\mathbf{K}.\mathbf{sgn}(\mathbf{s}(\xi))\right] d\xi. \tag{28}$$

Taking the first derivative of (28) yields

$$\dot{V}_2 = -\mathbf{e}^{\mathrm{T}}\Lambda\mathbf{e} - \mathbf{s}^{\mathrm{T}}\mathbf{K}\cdot\mathbf{sgn}(\mathbf{s}). \tag{29}$$

The uniform continuity of $\dot{V}_2$ is examined by looking at the following equation

$$\ddot{V}_2 = -2\mathbf{e}^{\mathrm{T}}\Lambda\dot{\mathbf{e}} - \dot{\mathbf{s}}^{\mathrm{T}}\mathbf{K}\cdot\mathbf{sgn}(\mathbf{s}) - \mathbf{s}^{\mathrm{T}}\mathbf{K}\cdot\frac{d\mathbf{sgn}(\mathbf{s})}{dt}. \tag{30}$$

In accordance with [29, 30], the final term in (30) is guaranteed to be completely finite. Moreover in the light of Assumptions $4-5$, all the remaining terms in $\ddot{V}_2$ are bounded. Therefore, $\ddot{V}_2$ is assured to be bounded. Applying Barbalat's lemma [31], it is obvious that $\dot{V}_2 \to 0$ as $t \to 0$. As a result, not only $\mathbf{e}$ but also $\mathbf{s}$ are guaranteed to be asymptotically convergent to zero.

The proof is completely finished here. ∎

Remark 3. If $|s_i|$ is much greater than 1, $|s_i|^{\alpha}$ with $0 < \alpha < 1$ is much smaller than itself. In the transient state, $|s_i|$ is often much greater than 1, and therefore thanks to the presence of $-\mathbf{K}\cdot\mathbf{sgn}(\mathbf{s})$ in (19) instead of - $\mathbf{Ks}$ as in [11], the capability of keeping the controller's output, τ, in the linear range of the actuators is significantly heightened (see Figure 2). The ability of occurring actuator saturation of the former, hence, is noticeably smaller than that of the latter.

4. SIMULATIONS

In this section, to confirm both the correctness and efficiency of the proposed control method, two computer simulations for trajectory tracking of the WMR were performed via Matlab-Simulink tool. The actual parameters of the WMR are expressed in Table 1. A fact, however, is needed to highlight that there was no preliminary knowledge of the dynamic parameters of the WMR. This is the reason why the RBFNN was used so as to approximate the dynamic nonlinear function $\mathbf{f}(\mathbf{x})$ of this WMR.

Without loss generality, the unknown wheel slips between the floor and the driving wheels have been assumed as follows

$$\begin{bmatrix} \dot{\gamma}_{\mathrm{R}} & \dot{\gamma}_{\mathrm{L}} & \dot{\eta} \end{bmatrix} = [\sin t \quad 1.5\cos 0.75t \quad 0.5]. \tag{31}$$

The control gains were chosen as follows $\hat{\Gamma}(0) = 0.5,\ \hat{\Upsilon}(0) = 2$

$$\mathbf{K} = \begin{bmatrix} 3 & 0 \\ 0 & 3 \end{bmatrix},\ \Lambda = \begin{bmatrix} 5 & 0 \\ 0 & 5 \end{bmatrix},\ \alpha = \frac{1}{3},\ \kappa = 6 = 0.05,\ \mathrm{H} = 0.1,\ \mathrm{P} = 1.$$

The architecture of the RBFNN was determined as follows: 6 inputs, 20 hidden neurons, and 2 output nodes. The learning-rate matrix $\mathbf{Q} = 2\mathbf{I}_{\mathbf{2\times 2}}$. The initial values of the RBFNN weight matrix $\hat{\mathbf{w}}(0)$ were chosen randomly in the range of $(0, 1)$.

For comparative purposes, the computer simulations of [11] and [32] were respectively carried out in the two following examples.

Example 1. The target D was on a straight line with the following trajectory

$$\begin{cases} x_{\mathrm{D}} = 4 + 0.4t \\ y_{\mathrm{D}} = -0.5 + 0.3t. \end{cases} \tag{32}$$

The initial posture in the world frame O-XY was selected as

$$\left[\begin{array}{ccc} x_{\mathrm{M}}(0) & y_{\mathrm{M}}(0) & \theta(0) \end{array}\right] = \left[\begin{array}{ccc} 0(\mathrm{m}) & 0(\mathrm{m}) & 0(\mathrm{rad}) \end{array}\right]. \tag{33}$$

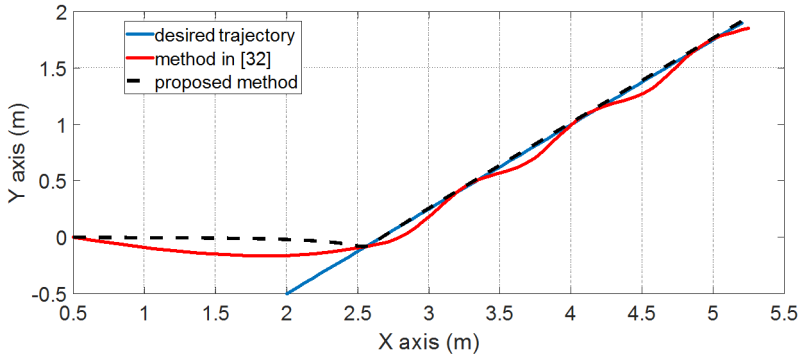

Figure 7. A comparison of tracking trajectories between two control methods in Example 1

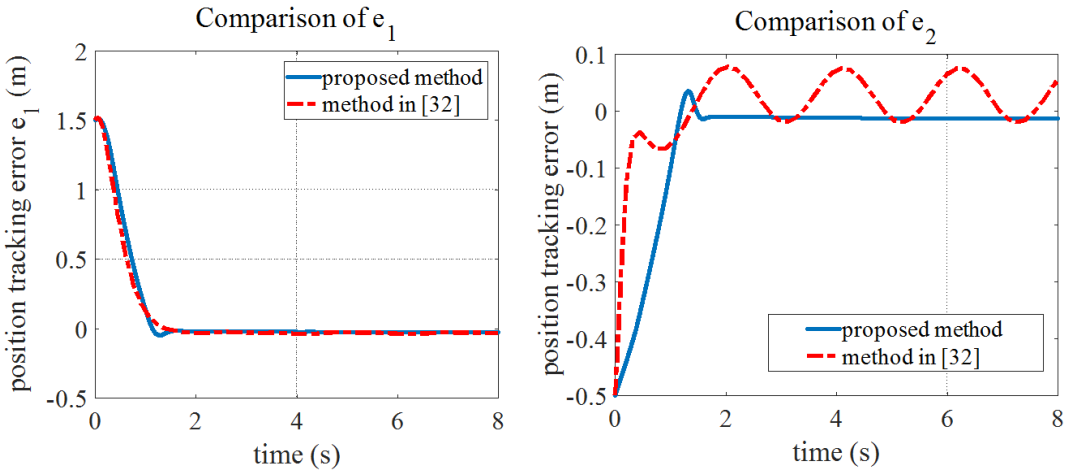

Figure 8. A comparison of the position tracking errors e between two control methods in Example 1

Figures 7, 8 and 9 depict the result of Example 1. Particularly, as can be seen from Figure 7, the proposed control method overcame the undesired influence of the unknown wheel slips more effectively than the one in [32]. The most striking feature in the steady state is that the greatest position tracking errors in the former were considerably smaller than those in the latter (see Figure 8), with $[|e_1|, |e_2|]^{\mathrm{T}} = \left[\begin{array}{cc} 0.025, & 0.013 \end{array}\right]^{\mathrm{T}}$ as opposed to $[|e_1|, |e_2|]^{\mathrm{T}} = \left[\begin{array}{cc} 0.041, & 0.07 \end{array}\right]^{\mathrm{T}}$ (m), respectively.

On the other hand, what stands out from Figure 9 is that the greatest torques (the controller's output), in the transient state, computed by the proposed control method are significantly smaller than those by the approach of [32], with the former constituting $\tau_{\max} = [24,\ 26]^{\mathrm{T}}$ and the latter $[152, -41]^{\mathrm{T}}$ (N.m). An explanation is Remark 3. For this reason,

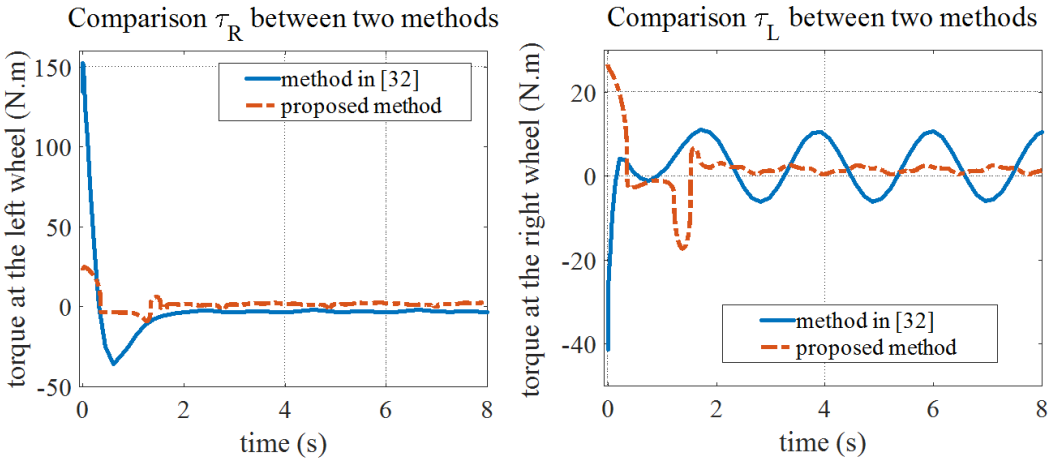

Figure 9. A comparison of torques between two control methods in Example 1

the capability of occurring actuator saturation of the former is much smaller than that of the latter.

Remark 4. Thanks to being designed in the body frame M-XY, our control method is more advantageous than that in [32] which was designed in the world frame O-XY.

Example 2. The target D was on a curved line with the following equation

$$\begin{cases} x_{\mathrm{D}} = 2 - 3\cos 0.2t + 0.1t \\ y_{\mathrm{D}} = 2 + 3\sin 0.2t - 0.1t. \end{cases} \tag{34}$$

For comparison, the computer simulations of both this proposed control method and the one in [11] were conducted.

The initial posture in the world frame O-XY was selected as

$$\begin{bmatrix} x_{\mathrm{M}}(0) & y_{\mathrm{M}}(0) & \theta(0) \end{bmatrix} = \begin{bmatrix} 0(\mathrm{m}) & 0(\mathrm{m}) & \dfrac{2\pi}{3}(\mathrm{rad}) \end{bmatrix}. \tag{35}$$

Figures 10, 11, 12 and 13 illustrated the comparative results of Example 2. Particularly, as can be seen from Figures 10 and 11 that the tracking control performances of our proposed control method and the approach in [11] are similar to each other. In contrast, the greatest computed torques by the proposed control method were also significantly smaller than those by [11] (see Figure 13), with the former constituting $\tau_{\max} = [14.2,\ 13.9]^{\mathrm{T}}$ and the latter $[81,\ 74]^{\mathrm{T}}$ (N.m).

Remark 5. So as to remove the chattering in $\mathbf{v_d}$ (the output of the kinematic controller), (14) is replaced by the following form

$$\mathbf{v}_{\mathrm{d}} = \begin{cases} \mathbf{h}^{-1}\left(-\Lambda\mathbf{e} - \begin{bmatrix} \cos\theta & \sin\theta \\ -\sin\theta & \cos\theta \end{bmatrix}\begin{bmatrix} \dot{x}_D \\ \dot{y}_D \end{bmatrix} - \hat{\Gamma}\dfrac{\mathbf{e}}{\|\mathbf{e}\|}\right) & \text{if } \|\mathbf{e}\| \geq \psi \\ \mathbf{h}^{-1}\left(-\Lambda\mathbf{e} - \begin{bmatrix} \cos\theta & \sin\theta \\ -\sin\theta & \cos\theta \end{bmatrix}\begin{bmatrix} \dot{x}_D \\ \dot{y}_D \end{bmatrix} - \hat{\Gamma}\dfrac{\mathbf{e}}{\psi}\right) & \text{if } \|\mathbf{e}\| \leq \psi, \end{cases} \tag{36}$$

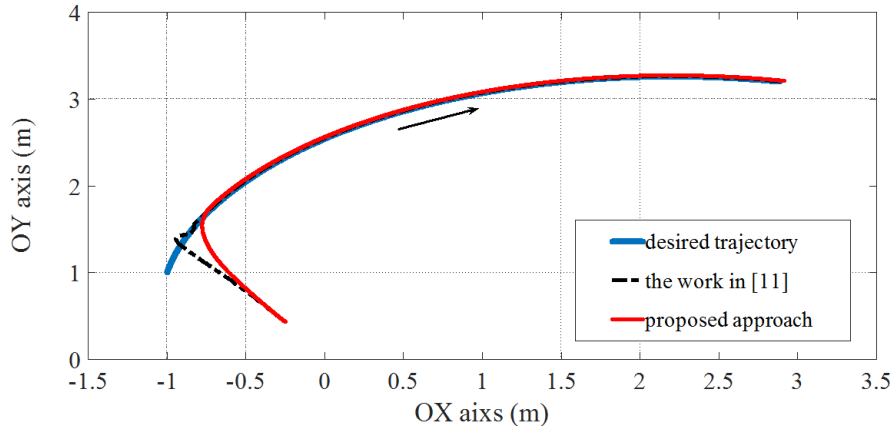

Figure 10. Another comparison of tracking trajectories in Example 2

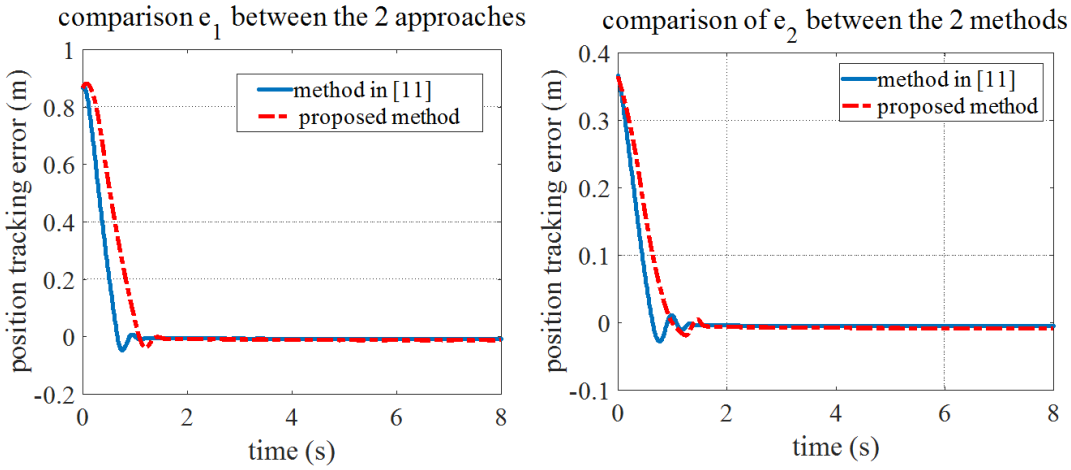

Figure 11. Another comparison of the position tracking errors e in Example 2

Table 1. The parameters of this WMR

symbol	Physical Meanings	Values
m_6	The mass of the WMR's platform	30(kg)
Ic	The platform's the inertial moment about the vertical axis crossing G	15.625 $(\mathrm{kg.m}^2)$
a	The length between G and M (see Figure 3)	0.2(m)
c	The length between P and M (see Figure 5)	0.5(m)
$\mathrm{m_W}$	each driving wheel's mass	2(kg)
$\mathrm{I_W}$	The inertial moment of each driving wheel about the rotation axis	0.0025 $(\mathrm{kg}, \mathrm{m}^2)$
$\mathrm{I_D}$	each driving wheel's inertial moment about its diameter axis	0.005 $(\mathrm{kg}, \mathrm{m}^2)$
b	half-distance of the wheel shaft	0.3(m)
r	The radius of each driving wheel	0.15(m)

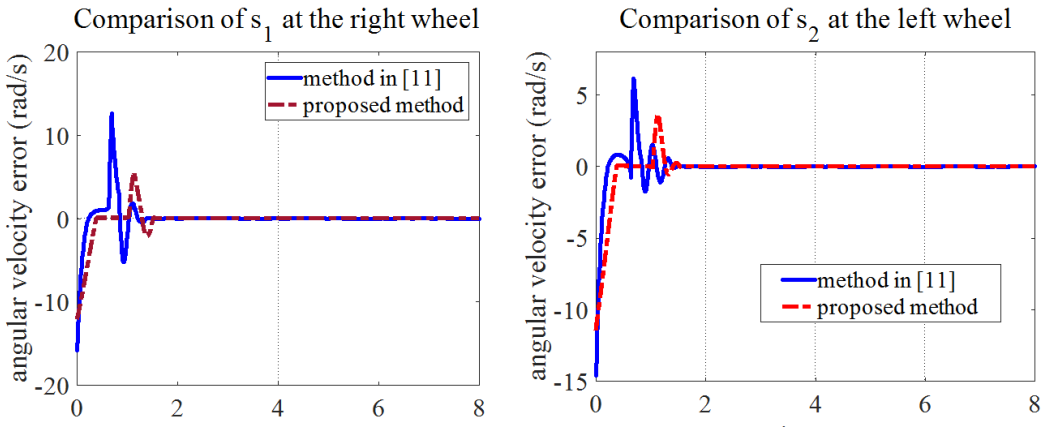

Figure 12. A comparison of the velocity tracking errors s in Example 2

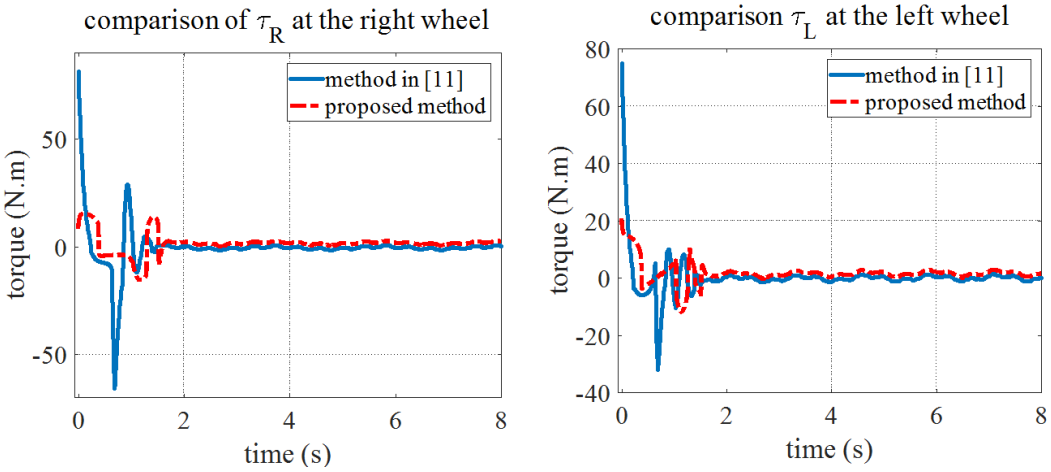

Figure 13. Another comparison of torques between two control methods in Example 2

where ψ is the value of a small positive real constant indicating a boundary layer around zero and can be chosen arbitrarily.

Remark 6. Likewise, to suppress the chattering of the dynamic control law τ in (19), the replacement of (19) will be conducted by the equation

$$\boldsymbol{\tau} = \begin{cases} -\mathbf{K} \cdot \mathbf{sgn}(\mathbf{s}) - \hat{\mathbf{f}}(\mathbf{x}) - \hat{\gamma}\dfrac{\mathbf{s}}{\|\mathbf{s}\|} & \text{if } \|\mathbf{s}\| \geq \kappa \\ -\mathbf{K} \cdot \mathbf{sgn}(\mathbf{s}) - \hat{\mathbf{f}}(\mathbf{x}) - \hat{\gamma}\dfrac{\mathbf{s}}{\kappa} & \text{if } \|\mathbf{s}\| < \kappa, \end{cases} \tag{37}$$

where κ is the value of a very small positive constant describing a boundary layer around zero and can be selected arbitrarily.

Last but not least, Figure 14 illustrates the comparison of torques of our proposed control

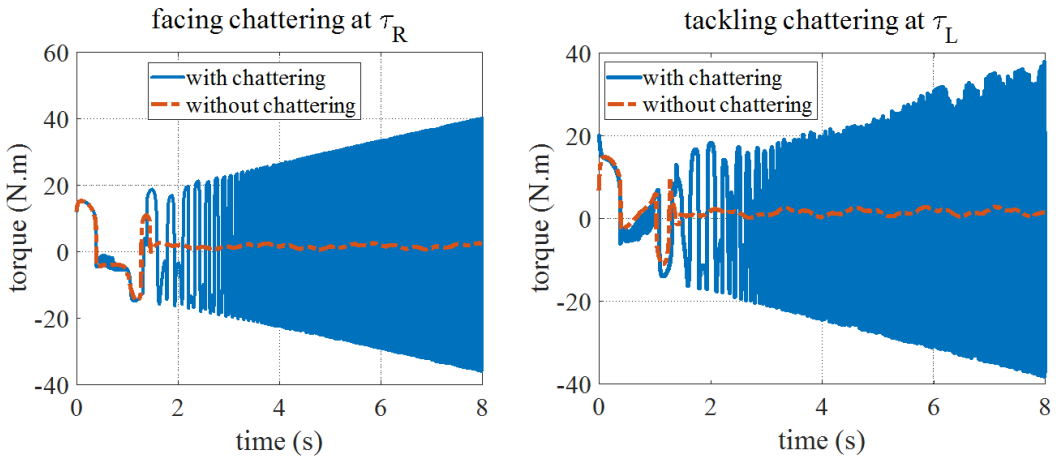

Figure 14. The bad effect of the chattering

method in Example 2 between with and without chattering (see Remarks 5-6). Of course, avoiding chattering allows the proposed control system to protect actuators and to save energy.

5. CONCLUSIONS

In this article, a novel robust tracking control scheme for actuator saturation has been proposed for a WMR in the presence of slippage and model uncertainties. Thanks to this control method, the asymptotic convergence of the tracking errors, namely both $\mathbf{e}$ and $\mathbf{s}$, to zero was guaranteed. The comparative simulation results have validated the correctness and efficiency of this proposed control scheme. In future, the strictly mathematical proof of the avoiding actuator saturation (see Remark 3) will be carried out.

ACKNOWLEDGEMENT

This work was supported by Institute of Information Technology, Vietnam Academy of Science and Technology, Hanoi, Vietnam, CS20.12.

REFERENCES

[1] L. Xin, Q. Wang, J.She, Y. Li, "Robotics and autonomous systems robust adaptive tracking control of wheeled mobile robot," *Robotics and Autonomous Systems,* vol. 78, pp. 36–48, 2016. https://doi.org/10.1016/j.robot.2016.01.002

[2] Y. Li, Z. Wang, and L. Zhu, "Adaptive neural network PID sliding mode dynamic control of nonholonomic mobile robot," *The 2010 IEEE International Conference on Information and Automation,* Harbin, 2010, pp. 753–757.

[3] D. Chwa, "Sliding-mode tracking control of nonholonomic wheeled mobile robots in polar coordinates," in *IEEE Transactions on Control Systems Technology,* vol. 12, no. 4, pp. 637–644, July 2004.

[4] D.H. Kim, J.H. Oh, "Tracking control of a two-wheeled mobile robot using inputoutput linearization," *Control Engineering Practice*, vol. 7, no. 3, pp. 369–373, 1999.

[5] Z. Hou, A. Zou, L. Cheng and M. Tan, "Adaptive control of an electrically driven nonholonomic mobile robot via backstepping and fuzzy approach," in *IEEE Transactions on Control Systems Technology*, vol. 17, no. 4, pp. 803–815, July 2009.

[6] N. Sidek and N. Sarkar, "Dynamic modeling and control of nonholonomic mobile robot with lateral slip," *Third International Conference on Systems (icons 2008)*, Cancun, 2008, pp. 35–40.

[7] Nguyen T, Le L, "Neural network-based adaptive tracking control for a nonholonomic wheeled mobile robot with unknown wheel slips, model uncertainties, and unknown bounded disturbances," *Turkish Journal of Electrical Engineering & Computer Sciences,* vol. 26, no. 1, pp. 378–392, 2018. Doi:10.3906/elk-1705-167

[8] Nguyen T, et al., "Neural network-based adaptive sliding mode control method for tracking of a nonholonomic wheeled mobile robot with unknown wheel slips, model uncertainties, and unknown bounded external disturbances," *Acta Polytechnica Hungarica*, vol. 15, no. 2, pp. 103–123, 2018.

[9] Nguyen T, Le L, "Neural network-based adaptive tracking control for a nonholonomic wheeled mobile robot subject to unknown wheel slips," *Journal of Computer Science and Cybernetics,* vol. 33, no. 1, pp. 1–17, 2017.

[10] Nguyen T, "Researching and developing some control laws for a wheeled mobile robot in the presence of slippage," Ph.D. Thesis, Graduate University of Science and Technology, VAST, 2018.

[11] Nguyen T, et al., "A gaussian wavelet network-based robust adaptive tracking controller for a wheeled mobile robot with unknown wheel slips," *International Journal of Control,* vol. 92, no. 11, pp. 2681–2692, 2019.

[12] H. Gao, et al., "Adaptive motion control of wheeled mobile robot with unknown slippage," *International Journal of Control,* vol. 87, no. 8, pp. 1513–1522, 2014.

[13] H. Fang, et al., "Trajectory tracking control of farm vehicles in presence of sliding," *Robotics and Autonomous Systems,* vol. 54, no. 10, pp. 828–839, 2006.

[14] J.C. Ryu, S.K. Agrawal, "Differential flatness-based robust control of mobile robots in the presence of slip," *The International Journal of Robotics Research*, vol. 30, no. 4, pp. 463–475, 2011. https://doi.org/10.1177/0278364910385586

[15] S.J. Yoo, "Approximation-based adaptive control for a class of mobile robots with unknown skidding and slipping," *International Journal of Control, Automation and Systems*, vol. 10, no. 4, pp. 703–710, 2012.

[16] S.J. Yoo, "Adaptive neural tracking and obstacle avoidance of uncertain mobile robots with unknown skidding and slipping," *Information Sciences,* vol. 238, pp. 176–189, 2013.

[17] H.S. Kang, et al., "Generalized extended state observer approach to robust tracking control for wheeled mobile robot with skidding and slipping," *International Journal of Advanced Robotic Systems*, vol. 10, no. 3, pp. 1–10, 2013.

[18] Y. Tian Y, N. Sarkar, "Control of a mobile robot subject to wheel slip," *Journal of Intelligent & Robotic Systems,* vol. 74, pp. 915–929, 2014.

[19] H. F. Grip, L. Imsland, T. A. Johansen, J. C. Kalkkuhl, and A. Suissa, "Vehicle sideslip estimation," in *IEEE Control Systems Magazine,* vol. 29, no. 5, pp. 36–52, Oct. 2009.

[20] R. Lenain et al., "Mixed kinematic and dynamic sideslip angle observer for accurate control of fast off-road mobile robots," *Journal of Field Robotics, Special Issue: VehicleTerrain Interaction for Mobile Robots,* vol. 27, no. 2, pp. 181–196, 2010.

[21] L. Li, F.Y. Wang, and Q. Zhou, "Integrated longitudinal and lateral tire/road friction modeling and monitoring for vehicle motion control," in *IEEE Transactions on Intelligent Transportation Systems,* vol. 7, no. 1, pp. 1–19, March 2006.

[22] H. Khan, J. Iqbal, K. Baizid, et al., "Longitudinal and lateral slip control of autonomous wheeled mobile robot for trajectory tracking," *Frontiers Inf Technol Electronic Eng,* vol. 16, pp. 166–172, 2015. https://doi.org/10.1631/FITEE.1400183

[23] J. Dakhlallah, S. Glaser, S. Mammar, and Y. Sebsadji, "Tire-road forces estimation using extended Kalman filter and sideslip angle evaluation," *2008 American Control Conference*, Seattle, WA, 2008, pp. 4597–4602.

[24] M. Kanamori, T. Saga, "Optimization of anti-windup for nonlinear systems with actuator saturation," *IFAC-PapersOnLine,* vol. 50, no. 1, pp. 747–752, 2017.

[25] J.O. Jang, "Neuro-fuzzy networks saturation compensation of DC motor systems," *Mechatronics,* vol. 19, no. 4, pp. 529–534, 2009.

[26] Z.S. Li, X.Q. Mo, S.J. Guo, et al., "4-degree-of-freedom anti-windup scheme for plants with actuator saturation," *Journal of Process Control,* vol. 47, pp. 111–120, 2016.

[27] A. Saberi, Zongli Lin, and A. R. Teel, "Control of linear systems with saturating actuators," in *IEEE Transactions on Automatic Control,* vol. 41, no. 3, pp. 368–378, March 1996.

[28] M.C. Turner, M. Kerr, "A nonlinear modification for improving dynamic anti-windup compensation," *European Journal of Control,* vol. 41, pp. 44–52, 2018.

[29] L. Wang, T. Chai and L. Zhai, "Neural-network-based terminal sliding-mode control of robotic manipulators including actuator dynamics," in *IEEE Transactions on Industrial Electronics*, vol. 56, no. 9, pp. 3296–3304, Sept. 2009.

[30] K. Nguyen, et al., "Adaptive antisingularity terminal sliding mode control for a robotic arm with model uncertainties and external disturbances," *Turkish Journal of Electrical Engineering & Computer Sciences,* vol. 26, pp. 3224–3238, 2018. Doi:10.3906/elk-1711-137

[31] J.J.E. Slotine, W. Li, et al., *Applied Nonlinear Control.* Prentice Hall Englewood Cliffs, NJ, 1991.

[32] N.B. Hoang, H.J. Kang, "Neural network-based adaptive tracking control of mobile robots in the presence of wheel slip and external disturbance force," *Neurocomputing,* vol. 188, pp. 12–22, 2016. https://doi.org/10.1016/j.neucom.2015.02.101

Received on February 05, 2020
Revised on April 12, 2020